Rev. int. hautes Tempér. Réfract., Fr., 1980, vol. 17, pp. 7-22.

Chemical engineering with CVD(*)

G. Wahl (1), R. Hoffmann (2)

(1) Brown Boveri & Cie AG, Zentrales, Forschungslabor, 6900 Heidelberg (R.F.A.)
(2) Brown Boveri & Cie AG 4600, Dortmund (R.F.A.)

Résumé. *Génie chimique en CVD.* Les problèmes hydrodynamiques dans les réacteurs CVD, petits ou très grands, sont discutés. Ils comprennent : le maintien de l'atmosphère du réacteur, le contrôle de l'écoulement des impuretés et l'optimisation de la composition des gaz afin d'obtenir les revêtements CVD convenables.

Les méthodes suivantes pour étudier ces problèmes sont décrites :

1) Calculs des débits gazeux et des dépôts.

2) Etudes expérimentales au moyen de fumées.

Ces différentes méthodes d'investigation sont appuyées par des mesures de dépôts de tungstène ($WF_6 + 3\ H_2 \rightarrow W + 6\ HF$) et de nitrure de silicium ($4\ NH_3 + 3\ SiH_4 \rightarrow Si3N_4 + \ldots$).

Summary. Hydrodynamic problems in small and large CVD-reactors are discussed. They encompass the compensation of the gas atmosphere in CVD-reactors, impurity flows, and optimal gas compositions as used for coating components. The following methods of investigating these problems is described :

1) Calculations of gas flow and deposition,

2) Fume experiments.

These investigations were supported by deposition measurements employing coatings of tungsten ($WF_6 + 3\ H_2 \rightarrow W + 6\ HF$) and Si_3N_4 ($4\ NH_3 + 3\ SiH_4 \rightarrow Si_3N_4 + \ldots$) coatings.

Introduction

CVD-processes in metallurgy may be considered a special group of heat treatment processes. All heat treatment processes require optimal gas flow conditions in order to achieve optimal deposition characteristics (thickness, crystal structure, adhesion). In addition the study of gas flow, particulary with respect to CVD-processes, is essential for the following reasons :

1) Most CVD-processes work with poisonous gases (CO, Cl_2, HF, F_2 HCl . . .). In order to minimize the consumption of these gases it is desirable to reach a high efficiency of the CVD-process, i.e. optimal flow conditions ;

2) today most CVD-processes are carried out in small reactors ($\cong 1\ m^3$). For the construction of larger CVD-reactors an exact study of the chemical kinetics and the hydrodynamics is mandatory.

Figures 1 and 2 demonstrate photographically and schematically a pusher type furnace which is mainly used for conventional heat treatment (carburizing). The work pieces to be treated are put on trays which are transported through the furnace. Entry and exit sections are constructed as lock chambers. The gas inlet for the main gas stream (endogas) is located in the upper part of the furnace at the points marked in *Figure 2*. The reaction gas (propane) is introduced at the points A, B and C. At these locations radial fans are mounted in order to level out the furnace atmosphere. From the gas inlet the gas streams

(*) Communication présentée à la *2e Réunion Européenne CVD : "Metallurgical Application of CVD"*, (Heidelberg 2-4 Avril 1979).

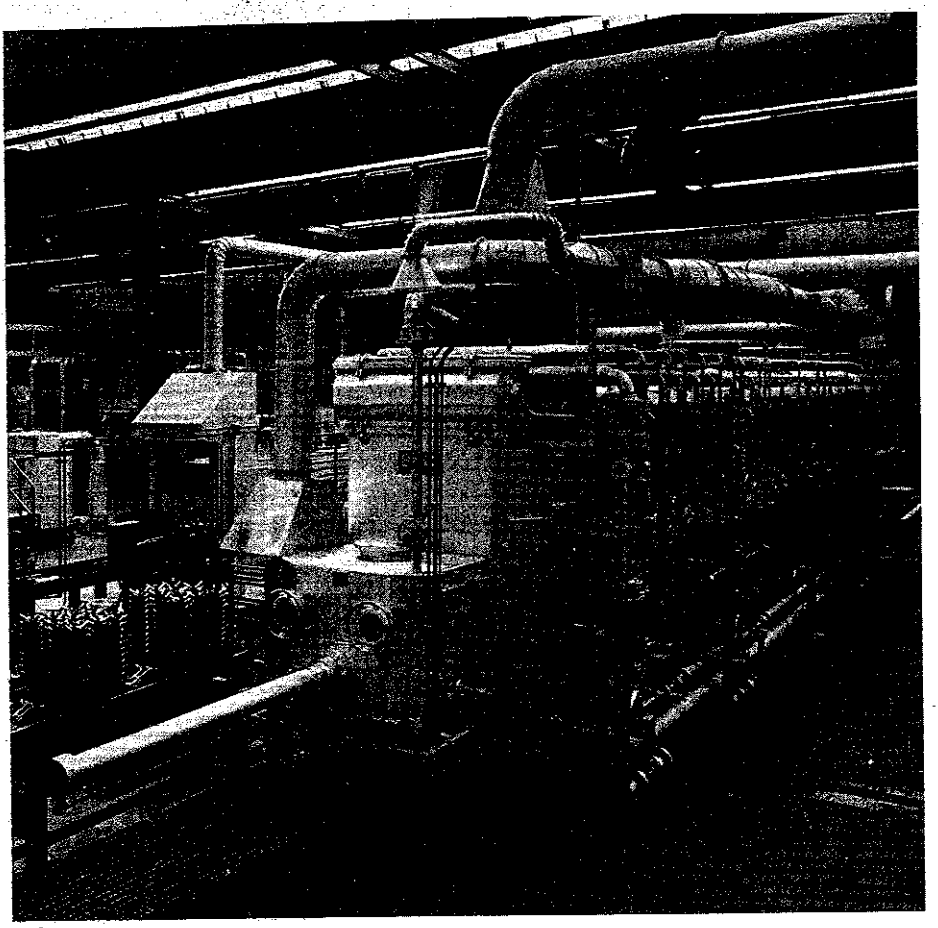

FIG. 1. – *Pusher-typ furnace for carburizing.*
FIG. 1. – *Four à poussoir pour carburation.*

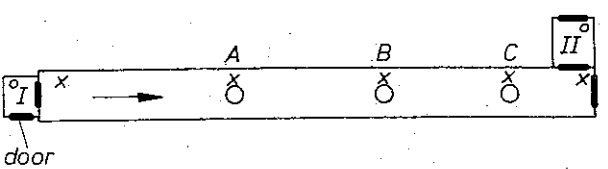

FIG. 2. – *Schematic of a pusher-type furnace. O Radial fans ; o exits of the gas ; x entry of dilution gas (or in the case of carburization endogas) ; I, II lock chambers ; ABC gas inlet of propane. Total length about 10 m.*
FIG. 2. – *Schéma du four à poussoir. o : Ventilateur. I, II : Sas ; A, B, C : Entrées de propane.*

through the exit and entrance sections into the environmental atmosphere. The following problems can be treated by hydrodynamic considerations :

1) The size, power and placement of the fans ;

2) The optimal flow pattern which minimizes the penetration of impurities into the furnace during the periods of charge and discharge (open doors) ;

3) Optimal flow conditions for every kind of loading.

Some of these problems have been solved for conventional heat treatment processes, but have to be discussed anew for CVD-applications.

The following gives an introduction on the hydrodynamic description of CVD-processes.

2. Fundamentals

The flow conditions in a chemical reactor are described by different characteristic numbers [2] :

1) *Reynolds number* $\mathrm{Re} = \rho v_o \ell / \eta_o$ (1)

(η_o = viscosity, v_o = gas velocity, ρ_o = density, ℓ = typical length). The subscript "o" means that a value typical of the flow system is taken.

2) *Froude number* $\mathrm{Fr} = v_o^2 / g\ell$ g = gravity (2)

3) *Prandtl number* $\mathrm{Pr} = \eta_o c_{p_o} / \lambda$ (3)

(c_{p_o} = specific heat at constant pressure, λ_o = heat conductivity).

4) *Schmidt number* $\mathrm{Sc} = \eta_o / \rho_o D_o$ (4)

(D_o = diffusion coefficient in the gas).

5) *The Mach number* $\mathrm{Ma} = v_o / v_c$ (5)

(v_c = velocity of sound).

6) It is possible to define numbers which characterize the chemical reactions in the gas and on the walls. One example of such a number is the Damköhler number Da. For a surface reaction of the order r ($j_1 = k_1 n_{SA}^r$, j_1 : surface reaction rate, n_{SA}^r : concentration of component A near the surface), the *Damköhler number* is defined by [3]

$$\mathrm{Da} = \frac{k_1 \ell}{D} n_{SA}^{r-1}. \tag{6}$$

For a homogeneous reaction ($j_2 = k_2 n_A^r$, j_2 : volume reaction rate) the Damköhler number is given by [3]

$$\mathrm{Da} = \frac{k_2 \ell^2}{D} n_A^{r-1}. \tag{7}$$

Most CVD-processes are governed by complicated reaction mechanisms, which make the definition of these chemical numbers very difficult.

From these numbers additional numbers can be derived which are often used for the description of hydrodynamical systems :

1) *Grashof number*

$$\mathrm{Gr} = g\rho_o \Delta\rho_o \ell^3 / \eta^2 = \frac{\mathrm{Re}^2}{\mathrm{Fr}} \frac{\Delta\rho_o}{\rho_o} \tag{8}$$

g = gravity, $\Delta\rho_o$ = typical density difference in the reactor.

If the difference $\Delta\rho_o$ is caused by temperature differences ΔT_o, $\Delta\rho_o$ can be correlated with the temperature difference by $\Delta\rho_o = \rho_o \Delta T_o / T_o$ (ρ_o : density at T_o).

2) *Rayleigh number:* $Ra = Pr \cdot Gr$ (9)

3) *Thiele number* [4] $Th = \sqrt{Da}$ (10)

In order to calculate these numbers the gas properties η, λ, D, c_p, v_c and the reaction constants must be known. The reaction constants must mostly be determined experimentally, whereas η, λ, D, c_p and v_c can be calculated [5] from the properties of the components. If these are not known, then values can be calculated from the critical data (critical temperature, critical pressure and critical compressibility [5]). *Figure 3* depicts the gas properties of a WF_6-H_2-mixture, whereby the heat conduction λ is calculated by the Mason-Saxena-Method [5,6], the viscosity by the Wilke [6,7] method and the diffusion coefficient by the kinetic gas theory (eq. 11-10 in [5]).

The flow pattern in a reaction chamber depends on the numbers mentioned above. Although there is generally an interdependence between the flow pattern and the CVD-process, gas flow and deposition process can be considered separately if the concentrations of the reacting components or the reaction rates are small.

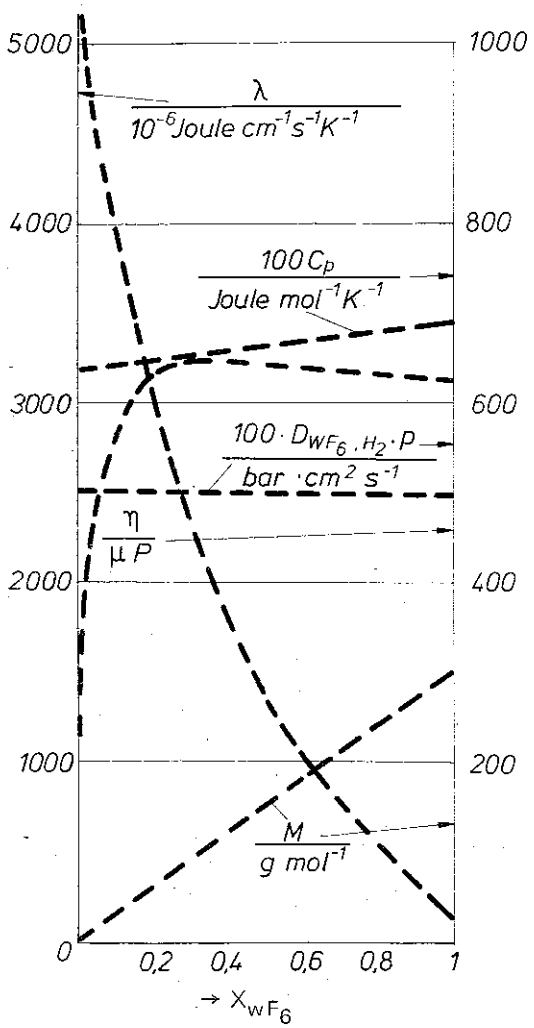

FIG. 3. – *The heat conduction λ (calculated by the Mason Saxena Method [5,6], the viscosity η (calculated by the Wilke-method [5,7], the binary diffusion coefficient D_{WF_6,H_2} (calculated by kinetic gas theory) eq. 11-10 in [5] and the molare heat in a WF_6-H_2-mixture. X_{WF_6} : molare fraction of WF_6. T = 1 400 K, p : total pressure.*

FIG. 3. – *La conduction thermique λ. La viscosité η. Le coefficient de diffusion binaire, en fonction de x_{WF_6}*

In most cases the gas flow patterns in the reactors are very complicated because the flow is driven by pressure differences (forced convection) and gravity (free convection). The competition between forced and free convection is decribed by the ratio $C = Gr/Re^2$ [2,8,9]. For small C forced and for large C free convection is predominant. Intermediately a regime exists – the so called combined flow regime – where the influence of both is predominant : in a horizontal reactor filled with N_2 the boundary between forced and combined convection was found to be at $Gr/Re^2 = 0.8 \ldots 3.5$ [8]. As to the boundary layer flow of gases with $Pr = 0.7$ like Ar, O_2, N_2, the following boundaries were cacula-ted [9] :

$$\begin{aligned} 0 &< \frac{Gr}{Re^2} < 0{,}3 && \text{forced convection} \\ 0{,}3 &< \frac{Gr}{Re^2} < 16 && \text{combined convection} \\ 16 &< \frac{Gr}{Re^2} && \text{free convection,} \end{aligned} \qquad (11)$$

where gravity supports the gas flow. For the opposing gas flow the boundaries :

$$\begin{aligned} 0 &< \frac{Gr}{Re^2} < 0{,}3 && \text{forced convection,} \\ 0{,}3 &< \frac{Gr}{Re^2} < && \text{combined convection} \end{aligned}$$

were calculated, but no criterion for free convection could be given by Sparrow [9]. The distance from the leading edge was taken as geometric parameter ℓ.

The predominance of the turbulent or the laminar flow at the forced convection can be estimated by the Reynolds number.

As far as free convection is concerned the Grashof or Rayleigh number gives information about the gas flow pattern. *Figure 4* shows the gas flow patterns [10] for gases and fluids between two infinite, horizontal plates at a distance d (taken as typical length for the calculation of Ra). The lower plate is heated up to the temperature T_b and the upper plate to the temperature $T_u < T_b$. At $g = 0$ no convection takes place in the enclosure regardless of the temperature difference $\Delta T = T_b - T_u$. This applies also to $g \neq 0$, provided that $T_u \geqslant T_b$. If, however, $T_u < T_b$, thermal convection can be caused by gravity. The convection can be either steady and 2 dimensional (laminar) or steady and 3 dimensional (laminar) or instationary and turbulent depending on the value of Ra. Dismukes *et al.* [11] estimated that most laboratory reactors used for Si deposition have values of Re and Gr in the ranges :

$$\begin{aligned} 1 &< Re < 300 \\ 50 &< Gr < 40\,000 \\ 10^{-3} &< \frac{Gr}{Re^2} < 1\,000 \end{aligned} \qquad (13)$$

Large reactors, such as are used in conventional heat treatment processes (volume $\geqslant \sim 1$ m^3 without fans) mostly have the following characteristic numbers.

$$\begin{aligned} &\sim 10 < Re < \sim 1\,000 \\ &Gr = 10^7 \ldots 10^{10} \\ \text{and } &10 < \frac{Gr}{Re^2} < 10^8. \end{aligned} \qquad (14)$$

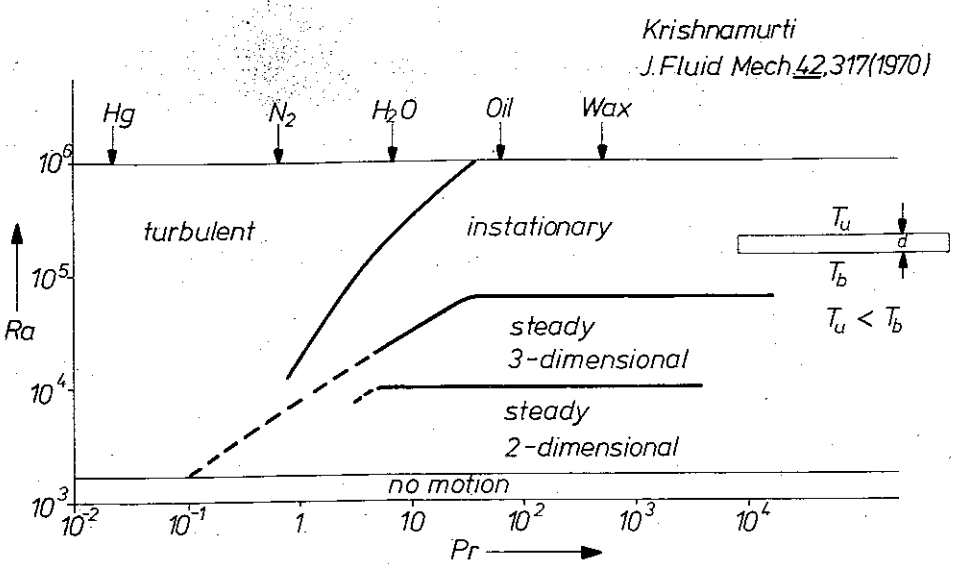

FIG. 4. – *Flow patterns in an enclosure for different fluids and gases* [10].
FIG. 4. – *Types d'écoulement entre deux plans parallèles horizontaux à températures T b, plus élevée que T u.*

For the calculation of Gr and Re the following values for v_o and ℓ were taken : ℓ_o : diameter of the furnace, v_o : gas velocity calculated from the gas inlet flow and the cross section of the furnace, temperature difference $\Delta T = 10°C$. Large reactors with fans work mostly in the forced convection region.

The Mach number Ma reveals the compressible qualities of the gas flow. As all reactors working at atmospheric pressure have values of $Ma << 1$, the influence of Ma can be neglected and the gas flow be considered as incompressible. In reactors working at low presures $Ma \sim 1$ can be reached.

3. Gas flow

3.1. Calculations. – All the laws governing the laminar gas flow are known, so that the gas flow can be calculated. For its calculation the continuity equation for the total mass, for the single components, for the energy and for the momentum must be solved [2,12,13]. Apart from this the boundary conditions on the walls must be taken into account.

Laminar gas flow calculations are not only useful for reactors in which the gas flow is laminar but also for turbulent reactors as they have laminar zones in small tubes and holes or between the working pieces, if the distances are small.

Calculations for turbulent conditions are very complicated and not always possible [14].

The following two examples explain the use of such gas flow calculations. In both examples flow and deposition can be separated. Therefore the gas flow can be treated regardless of the deposition :

1) In order to achieve gas flow-conditions without recirculation effects [2,15], the gas flow was studied in the reactor shown in *Figure 5* which was used for SiO_2 and Si_3N_4 deposition from SiH_4 and O_2 or NH_3 in N_2-dilution. The whole apparatus could

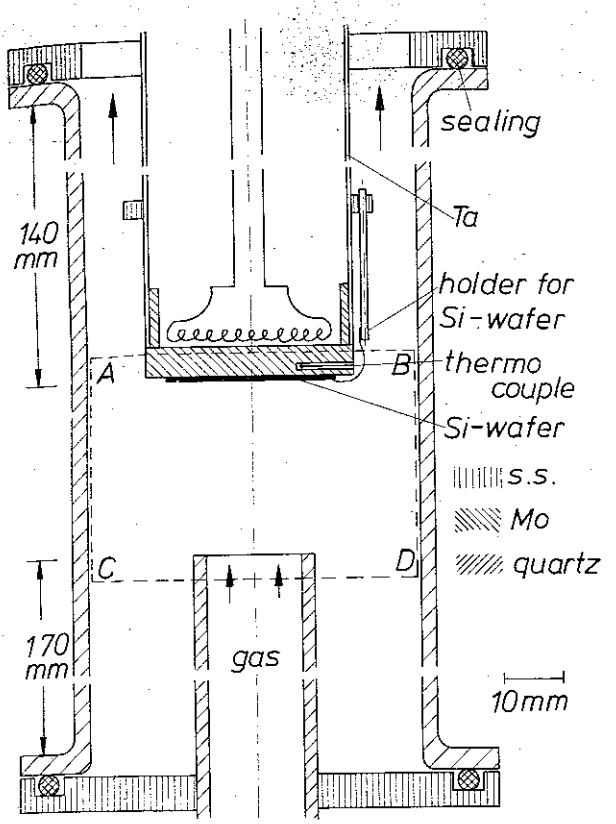

FIG. 5. – *Reactor geometry for Si_3N_4 and SiO_2 deposition [15]. ABCD see Figures 6, 7 and 10. s.s. : stainless steel.*
FIG. 5. – *Géométrie de réacteur pour le dépôt de Si_3N_4 ou de SiO_2 [15]. S.S. : acier inoxydable.*

be reversed. According to *Figure 6* and 7 gas flow without recirculation is possible, if buoyancy supports the forced convection. More flow patterns were calculated at different Re ($50 < Re < 250$) as well as different deposition temperatures ($300\ K < T_d < 1\ 300\ K$). The transition between forced convection and combined convection was found to take place at $Gr/Re^2 \approx 1$. For the calculation of Gr the distance between the deposition surface and the nozzle and for the calculation of Re the radius of the nozzle were taken as typical length ℓ.

2) Hydrodynamic calculations enable us to simultaneously calculate the gas flow and the diffusion of gases in order to produce reaction gases for CVD-processes as the following example [16] shows : *Figure 8* indicates the geometry of a reactor in which the deposition of Y_2O_3 and ZrO_2 was carried out by the reaction :

oxygen + chloride of metal → oxide.

O_2 was led through the ring tube and the chloride produced by direct chlorination of Y or Zr through the inner tube. Both gases must be mixed in order to produce the reaction gas.

The gas flow and the diffusion calculations were carried out under isothermal conditions because the temperature differences in the reactor were small ($\Delta T < 150°C$) in comparison with the deposition and chlorination temperature ($T = 800 - 1\ 000°C$).

Figure 8 shows the calculated stream lines for $Re = 20$ (calculated with the radius R of the inner tube) and the ratio $i_1/i_2 = 0.6$ (i_1 : gas flow through the inner tube, i_2 : gas flow through the outer tube). *Figure 9* shows the diffusion of O_2 from the outer

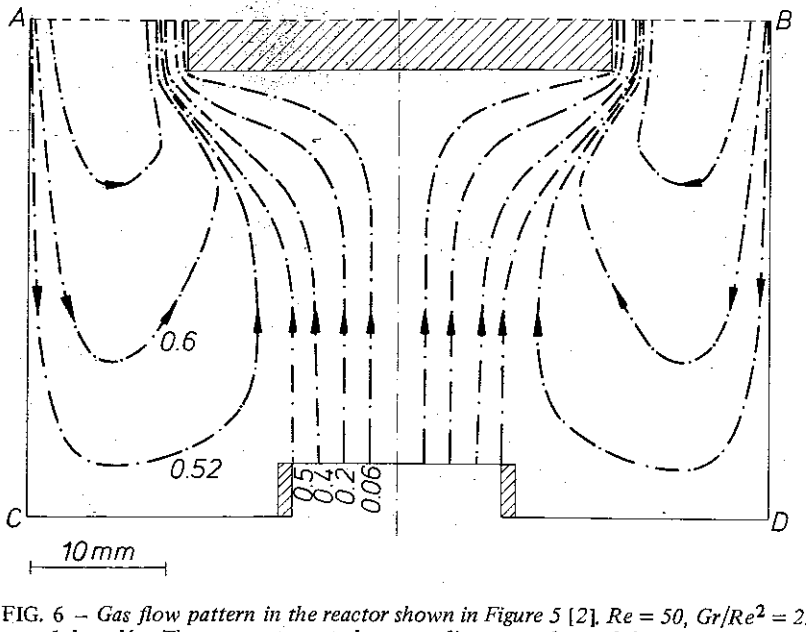

FIG. 6 – *Gas flow pattern in the reactor shown in Figure 5* [2]. *Re = 50, $Gr/Re^2 = 22$, $T_d = 600\,^{\circ}C$, $p = 1$ bar, N_2. The parameters at the streamlines are values of the reduced stream function $\psi^+ = \psi/v_o R^2 g_o$ (R : radius of the tube for the gas inlet).*

FIG. 6 – *Figuration de l'écoulement des gaz dans le réacteur 5.* [2].

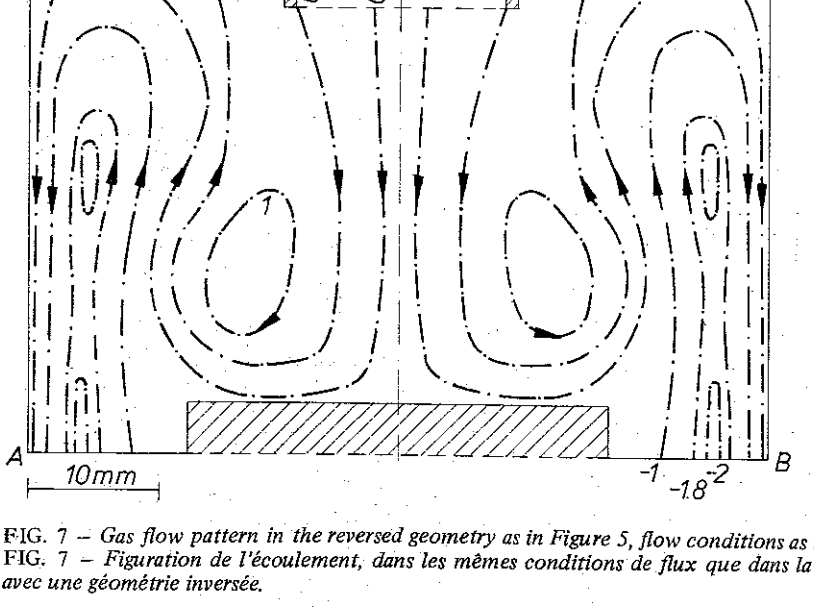

FIG. 7 – *Gas flow pattern in the reversed geometry as in Figure 5, flow conditions as in Figure 6* [2].

FIG. 7 – *Figuration de l'écoulement, dans les mêmes conditions de flux que dans la Figure 6, mais avec une géométrie inversée.*

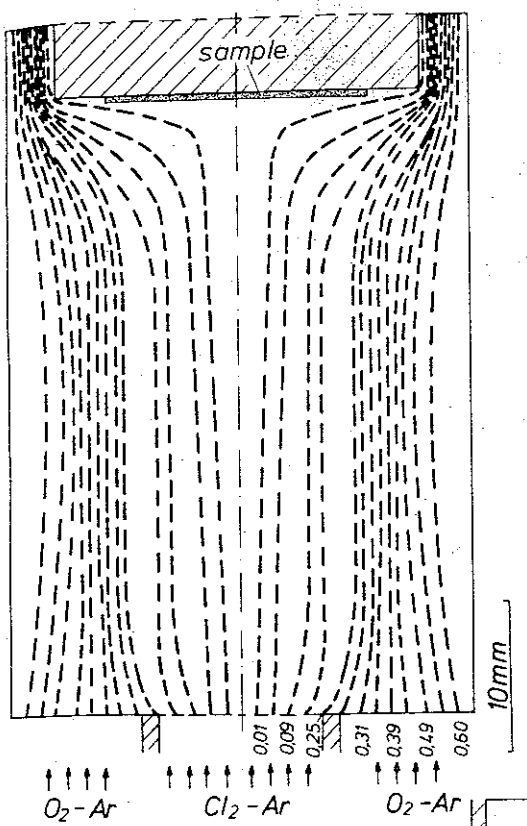

FIG. 8. – *Gas flow pattern in an axisymmetric reactor used for Y_2O_3 or Zro_2 deposition from chloride and oxygen [16]. Re = 20, $i_1/i_2 = 0.6$ [16].*

FIG. 8. – *Figuration de l'écoulement des gaz dans un réacteur axi symétrique, utilisé pour le dépôt de Y_2O_3 ou de Zro_2 à partir du chlorure métallique et d'oxygène [16].*

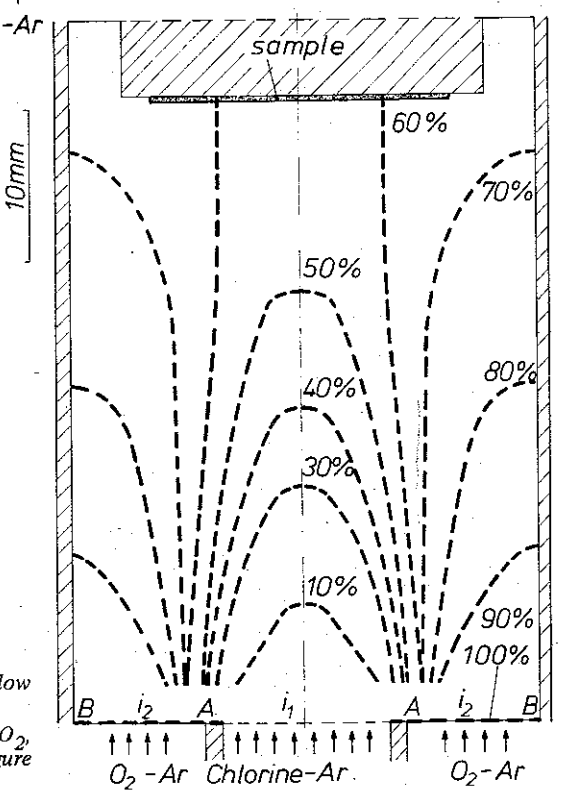

FIG. 9. – O_2-diffusion pattern [16]. *Gas flow conditions as in Figure 8.*

FIG. 9. – *Figuration de la diffusion de O_2, avec les mêmes conditions de flux que Figure 8.*

zones into the central gas flow. Parameter at the concentration lines is the reduced mole fraction $x^* = x^i_{o_2}/x^i_{o_2}$ ($x^i_{o_2}$ = mole fraction of O_2 at the gas inlet). No deposition on the walls was assumed. *Figure 9* shows that sufficient mixing between the chloride flow and the O_2-containing flow leads to oxide formation.

3.2. Visualization experiments. – One possibility of visualizing the gas flow are $TiCl_4$-H_2O-fume-experiments [8, 2]. In these experiments $TiCl_4$-vapor and H_2O-vapor react together and the formed oxide fume is observed by spot light. *Figure 10* and *11* show examples of fume experiments at flow conditions used for the calculations of *Figures 7* and *8*. Both figures demonstrate a good agreement between experiment and calculation.

Figure 11 and 12 show the influence of small deviations of the position of the sample on the gas flow. The calculation of the gas flow in *Figure 12* would be very extensive because the gas flow is not axisymmetric.

The advantage of fume experiments over the calculation method is, that these studies can be made even at very complicated reactor geometries, the main disadvantage being that the reactor must be transparent.

3.3. Deposition calculation. – Deposition calculations depend on the processes which control the deposition :

1) If the deposition is controlled by chemical reactions on the surface the methods of surface kinetics can be applied.

2) In contrast to (1) there are processes in which the mass-transport in the gas phase controls the deposition.

In the following the latter process is described. For the sake of simplicity the considerations are confined to depositions which are controlled by the transport of one

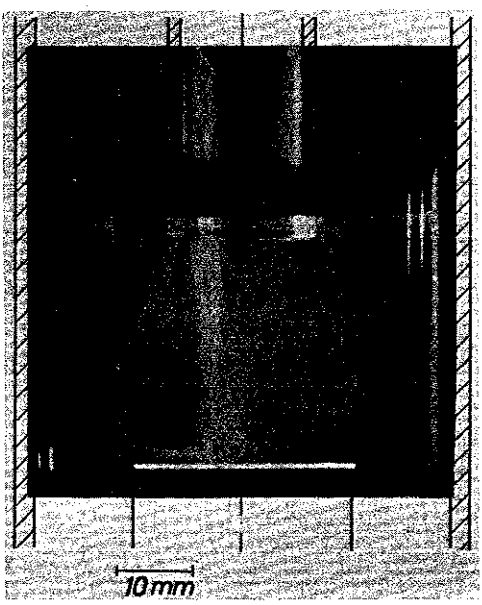

FIG. 10. – *Experimental flow pattern at the same flow conditions as in Figure 7* [2].
FIG. 10. – *Visualisation expérimentale de l'écoulement des gaz dans les mêmes conditions de flux que Figure 7* [2].

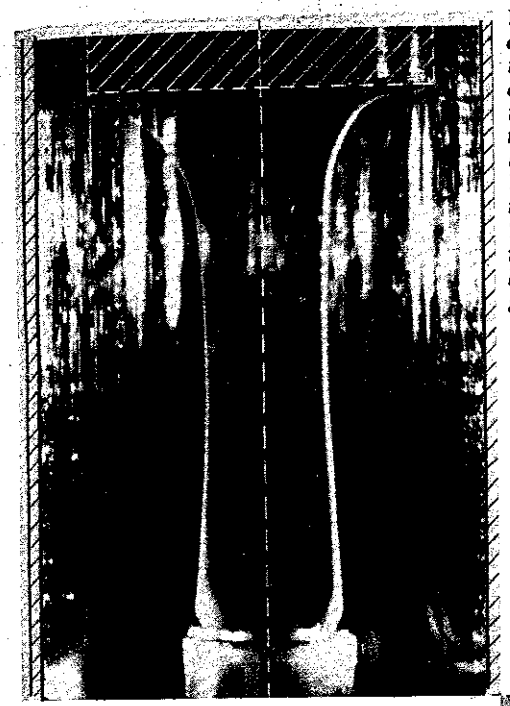

FIG. 11. – *Experimental flow pattern [16], flow conditions as in Figure 8. The lines on the picture are due to internal light reflections in the quartz tube. TiO_2 – fume was produced by reaction of $TiCl_4$ flowing in the inner tube and H_2O in the ring tube. Therefore only the boundary between both gas flows is visible.*

FIG. 11. – *Visualisation expérimentale dans les mêmes conditions que Figure 8. Des fumées de TiO_2 sont produites par réaction de $TiCl_4$ arrivant par le tube intérieur et de H_2O arrivant par le tube annulaire. Seule la frontière entre les deux gaz est visible.*

FIG. 12. – *Experimental flow pattern, conditions as in Figure 8 but the deposition surface is arranged oblique. $Ti\varphi_4$–H_2O in the inner tube.*

FIG. 12. – *Visualisation expérimentale du flux gazeux, conditions de la Figure 8, mais le substrat est placé obliquement.*

component B onto the surface. The flow is to be incompressible (Ma $\ll$ 1). To describe the deposition the Sherwood number is introduced [2,3].

$$Sh = \frac{\dot{m}_B \, \ell}{D \, \Delta \rho_B} \tag{15}$$

(m_B : local mass deposition rate, D : diffusion coefficient of component B in the gas, $\Delta\rho_B$: density difference of the density ρ_B of component B between the surface and the free flowing gas). This number is defined in analogy to the Nusselt number for the heat transfer :

$$Nu = \frac{\dot{q} \, \ell}{\Delta T \, \lambda} \tag{16}$$

($\dot{q}$: density of heat transfer to the surface, ΔT : temperature difference between the surface and the free flowing gas).

In general the Sherwood number depends on parameters mentioned in section 2 and on the parameters Q, η^*, λ^*, D^*, c_p^*, r_s^* [2]

$$Sh = f(r_s^*, Re, Sc, Pr, Fr, Q, \eta^*, \lambda^*, D^*, C_p^*) \tag{17}$$

with the ratio $Q = T_d/T_o$ (T_d : deposition temperature, T_o : temperature of the gas at the gas inlet), the reduced temperature dependent functions $\eta^* = \eta/\eta_o$, $\lambda^* = \lambda/\lambda_o$, $D^* = D/D_o$, $c_p^* = c_p/c_{p_o}$ and the dimensionless local surface parameter r_s^*.

If the influence of gravity can be neglected the eq. (17) can be simplified :

$$Sh = g(r_s^*, Re, Sc, Pr, \Omega, \eta^*, \lambda^*, D^*, c_p^*). \tag{18}$$

In this equation, in contrast to eq (17) all values except Re are pressure independent. Therefore at constant Re the Sherwood number Sh does not depend on pressure and the mass deposition rate

$$\dot{m}_B = \frac{D_o}{R_o} \Delta\rho_B \, g(r_s^*, Re, Sc, Pr, Q, \eta^*, \lambda^*, D^*, c_p^*) \tag{19}$$

is also pressure independent because D_o is $D_o \propto 1/p_o$.

If in addition the temperature differences are small, thus that the process is isothermal, the influence of Q, η^*, λ^*, D^* and c_p^* can be neglected :

$$Sh = h(r_s^*, Re, Sc). \tag{20}$$

Heat mass transfer analogies can only be applied in this case. The equivalent heat-transfer equation

$$Nu = h(r_s^*, Re, Pr). \tag{21}$$

which is in some cases known in the furnace technology [17].

Eq. (20) can be formed by the exchange of Nu and Pr, by Sh and Sc. Relations like (20) can be used approximately for deposition calculations if the conditions under which eq. 20 is correct are not fulfilled (large temperature differences, multicomponent diffusion processes). It is then necessary to use special approximation methods as developed by Carlton-Oxley [18].

Figure 13 shows the application of eq. 20 to the investigation of W-deposition [19] from a WF_6/H_2 – mixture by the reaction

$$WF_6 + 3H_2 \rightarrow W + 6\,HF$$

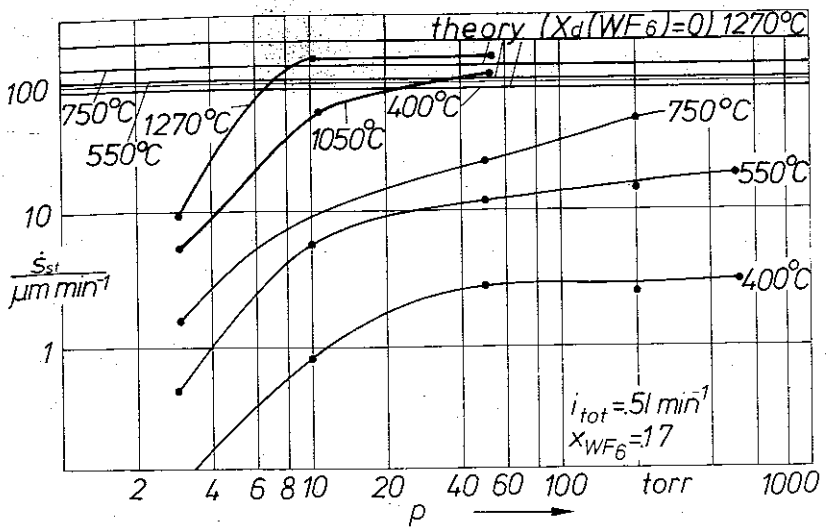

FIG. 13. – *Tungsten deposition rates in the stagnation point at different deposition temperatures T_d. Comparison of experimental with calculated values, x_d (WF_6) : molar fraction of WF_6 near the deposition surface* [19].
FIG. 13. – *Vitesse de dépôt du tungstène au point de stagnation pour différentes températures : Td. Comparaison entre valeurs expérimentales et calculées.* [19].

in a stagnation flow geometry. At the stagnation point the deposition can be described by the relation [2,16].

$$Sh_{St} = 0.6.\ Re^{1/2}\ Sc^{1/3}. \tag{22}$$

As the temperature differences were large (gas inlet temperature 300 K, deposition temperatures 800 – 1200 K) and the deposition process being determined by a multicomponent diffusion, the method of Carlton Oxley was used. In ranges where a mass transport controlled deposition can be expected (high pressure, high temperature) the accordance between experimental values and calculations is good. At low pressures and/or low temperature surface processes control the deposition.

If mass transfer formulae like eq. (17 ... 21) are not known, the mass transfer can be calculated

1) by application of boundary layer theories, if the gas flow far from the deposition surface is known [20,3] ;

2) by an exact calculation of the total gas flow and deposition problem [2].

Figure 14 shows the result of such deposition calculations according to the 2nd method by simultaneous solution of the equations mentioned in section 3. The Si_3N_4 deposition experiments were made in the reactor shown in *Figure 4* according to the reaction $3SiH_4 + 4NH_3 \rightarrow Si_3N_4 + \ldots$ *Figure 14* shows a good agreement of the experimental and calculated deposition profiles.

The absolute deposition rates s_{st} (*Figure 15*) can, however, only be fitted to the experimental values by introducing the fitting parameter, which takes into account surface kinetics effects :

$$\gamma = \frac{Y_o\,(SiH_4) - Y_d\,(SiH_4)}{Y_o\,(SiH_4)} \tag{23}$$

(Y_o (SiH_4) : mass fraction in the gas flow far from the surface, Y_d : assumed mass fraction near the surface ($o \leqslant \gamma \leqslant 1$)).

The profile as shown in *Figure 14* does not depend on γ. *Figure 15* shows that only in some ranges the calculated profiles agree with the experimental profiles.

If surface reactions control the deposition, Sh also depends on chemical numbers like Da. In order to see the influence of chemical reactions on the deposition, we will study the deposition on the walls of a hole (depth $L = \infty$, diameter d). The gas is assumed to be stagnant in the hole, so that the gas components are transported by diffusion from the opening into the hole. The deposition is to be governed by the law

$$j_B = k n_{SB},$$

where j_B is the deposition rate. Under the assumption that the concentrations $n_B = n_{SB}$ are constant over the cross section, the deposition rate j_B can be calculated by the differential equation :

$$\frac{\pi d^2}{4} D \frac{\partial^2 n_B}{\partial x^2} = \pi d k n_B \tag{24}$$

with the solution :

$$n_B = n_{B_o} \exp(-2\sqrt{Da}\, x/d) \tag{25}$$

(x : distance from the opening of the hole, $Da = k d/D$)

The distance $x_{1/2}$ from the opening, where the deposition rate has reached the value $1/2\, j_{B_o}$ (j_{B_o} = deposition rate at the opening), is

$$x_{1/2} = \frac{0{,}347}{\sqrt{Da}} d \tag{26}$$

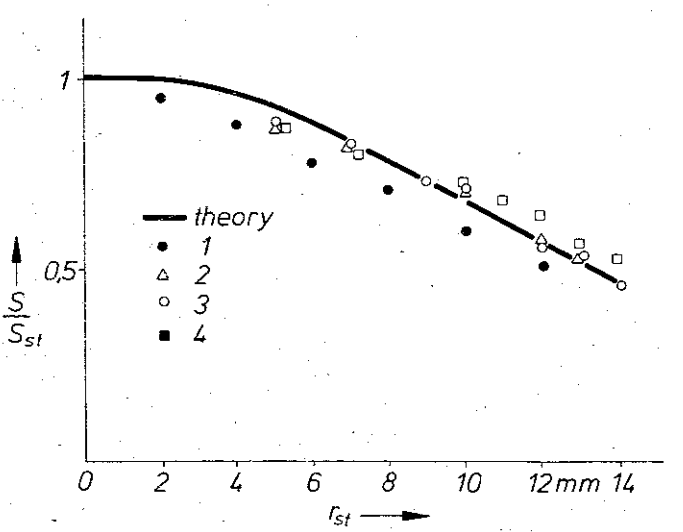

FIG. 14. – *Theoretical and experimental Si_3N_4 profiles. The numbers relate to the numbers on the measuring points in Figure 15. s : local thickness, s_{st} : thickness in the stagnation point, r_{st} : radial distance from the stagnation point* [2].

FIG. 14. – *Profil d'épaisseur du dépôt de Si_3N_4 (2). S épaisseur à la distance radiale r st S_{st} épaisseur au point de stagnation.*

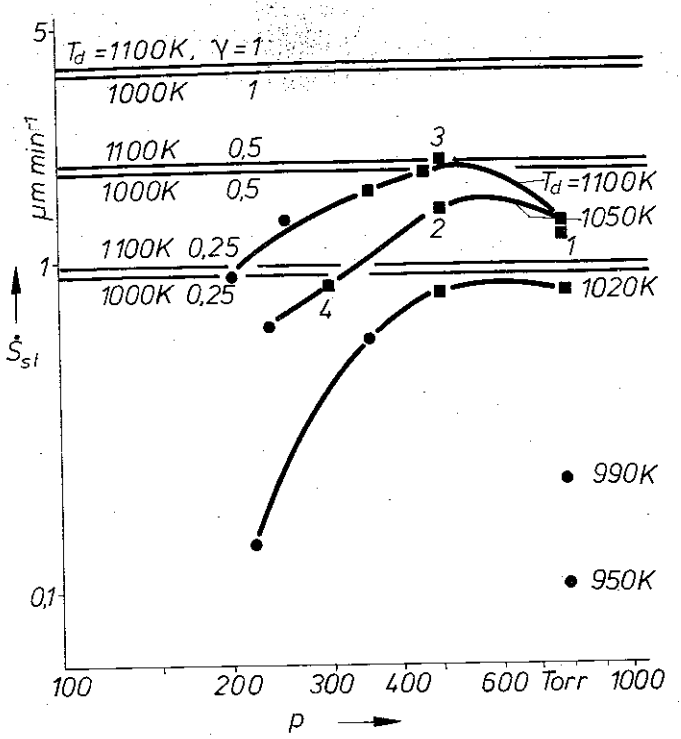

FIG. 15. – *Theoretical and experimental growth rates s_{st} of Si_3N_4 in the stagnation points vs. pressure p.* ■ *measured profile is in accordance with the calculated profile (Figure 14)* [2].
FIG. 15. – *Vitesses de croissance théoriques et expérimentales S_{st} de Si_3N_4 en fonction de p.*

For reactions of the order $r \neq 1$ ($j_B = k\, n_{SB}^r$) the result of a similar calculation is

$$x_{1/2} = \frac{1 - 2^{\frac{r-1}{2}}}{1 - r} \sqrt{\frac{1 + r}{2\,Da}}\, d \qquad (27)$$

Eqs. (26) and (27) show that $x_{1/2}$ increases with decreasing Da, that means, that a very slow reactions a deposition of deep tubes is possible. If the deposition is gas diffusion controlled, the length $x_{1/2}$ is approximately

$$x_{1/2} \sim \frac{d}{2}.$$

This example demonstrates that in the reaction controlled range the throwing power can be increased. Therefore a coating of complicated forms is easier and less dependent on flow conditions than in the diffusion controlled range.

Conclusions

The methods described show the possibilities of estimating the flow and the deposition in small and large reactors, if the chemical processes are only on the surface ; reactions in the gas flow, however, have been neglected in this paper. Hints that these processes can influence the deposition are known from CVD-processes [19]. The importance of

volume reactions increases in larger chemical reactors because, normally, the residence times of the gas in large reactors are larger than in small reactors. Therefore, if chemical reactions in flowing gas are existent, the kinetics of these processes must be investigated in addition in order to scale up reactors.

References

[1] Benninghoff (H.), Zickler (H.). – *Metalloberfläche*, 1978, *32*, 118.
[2] Wahl (G.). – *Thin Solid Films*, 1977, *40*, 13-26.
[3] Brauer (H.). – Stoffaustausch, Verl. *Sauerländer*, Frankfurt, 1971.
[4] Schlosser (E.G.). – Heterogene Katalyse, Verl. *Chemie*, 1972.
[5] Reid (R.C.), Sherwood (Th.K.). – The Properties of Gases and Liquids, *McGraw Hill*, New York, 1958.
[6] Mason (E.A.), Saxena (S.C.). – *Phys. Fluids*, 1958, *1*, 361.
[7] Wilke (C.R.). – *J. Chem. Phys.* 1950, *18*, 517.
[8] Takashashi (R.), Sugawara (K.), Nakazawa (Y.), Koga (Y.). – in Proc. 2. Int. CVD *Conf.* (eds. J.M. Blocher, J.C. Withers), *Electrochem. Soc.*, (Princeton), (1970) 695.
[9] Sparrow (E.M.). – *Phys. Fluids*, 1959, *2*, 319.
[10] Krishnamurti (R.). – *J. Fluid. Mech.*, 1970, *42*, 309.
[11] Dismukes (J.P.), Curtis (B.J.). – Proc. 2nd. Int. *Symp.* Silicon Science and Techn. (eds H.R. Huff, R.R. Burgess) *Electro-chem. Soc., (Princeton*, 1973).
[12] Gosmann (A.O.), Pun (W.M.), Runchal (W.M.), Spalding (D.B.), Wolfshtein (M.). – *Academic Press*, London, 1973.
[13] Mazille (J.E.). – *Thesis*, Grenoble, 1973.
[14] Launder (B.E), Spalding (D.B.). – Mathematical Models of Turbulence, *Academic Press*, London, 1972.
[15] Wahl (G.). – in Proc. 5th Int. *Conf.* on CVD, (eds. J.M. Blocher, H.E. Hintermann, L.H.), *Electrochem. Soc., Princeton*, 1975, 391.
[16] Wahl (G.). – in Proc. 7th Int. *Conf.* on CVD, (eds. H. Lydtin, Th. Sedgwick) *Electrochem. Soc. Princeton*, 1979, 536.
[17] Senkara (T.). – Wärmetechnische Rechnungen für gas- und oelbeheizte Wärmeöfen, *Vulkanverl.* Essen, 1977.
[18] Carlton (H.E.), Oxley (J.H.). – in Proc. Chem. Vap. Dep. of Refr. Met. Alloys and Compounds, (ed. AC Schaffhauser), *Amer Nucl. Soc.*, (Hinsdale), 1967, 19.
[19] Wahl (G.), Batzies (P.). – in Proc. 4th Int. CVD *Conf.*, (ed. G.F. Wakefield, J.M. Blocher), 1973, 425.
[20] Schlichting (H.). – Grenzschichttheorie, *Braun*, Verl., Karlsruhe, 1965.